Mechanical and electrical coupling at metal-insulator-metal nanoscale contacts

Doo-In Kim, Namboodiri Pradeep, Frank W. DelRio,[a] and Robert F. Cook
Ceramics Division, Materials Science and Engineering Laboratory, National Institute of Standards and Technology, Gaithersburg, Maryland 20899, USA

(Received 26 September 2008; accepted 6 October 2008; published online 18 November 2008)

Mechanical and electrical coupling at nanoscale metallic contacts was investigated using a conducting-probe atomic force microscope (AFM). The current-voltage responses were non-Ohmic, symmetric about zero bias, with conductance values smaller than the quantum conductance limit, which indicate electron tunneling through an insulating layer. Using a self-consistent contact mechanics model and a parabolic tunneling model for thin insulating layers, we determined the contact area, barrier height, and barrier thickness as a function of applied contact load. The results suggest the presence of *two* insulating layers: an oxide layer on the AFM tip and an organic contaminant layer on the metallic surface. © *2008 American Institute of Physics*.
[DOI: 10.1063/1.3009211]

Micro- and nanoscale mechanical contacts are anticipated to play a large role as electrical switches in advanced radio frequency[1,2] and microwave[3] communication devices and as electrical junctions in nanoelectronics applications.[4] For example, the superior performance characteristics of microelectromechanical systems (MEMS)-based switches relative to semiconductor-based switches, including linearity (i.e., Ohmic behavior), small insertion loss and power consumption, small size, and decreased cost, are expected to lead to their use in cellular phones for controlling power and switching between antenna banks.[1,2,5–7] The Ohmic conductance arises from large numbers of metal-metal junctions formed at contacts between asperities on the electrodes. Each asperity contact supports a load of ≈ 1 μN and contributes ≈ 10 mS to the conductance of the switch. Such contacts are well described by quasicontinuum models of conduction that include diffuse and ballistic electron motion through constrictions.[7,8] At the other extreme, atomic-scale metallic junctions exhibit discrete conductance values quantized in terms of $G_0 = 2e^2/h = 77$ μS, the quantum unit of conductance, where e is the electron charge and h is Planck's constant.[9,10] The characteristic contact load associated with such atomic-scale junctions is ≈ 1 nN, the force required to break a single atomic bond. Nanoelectromechanical systems switches and junctions utilize contact loads between the ≈ 1 μN of MEMS devices and the ≈ 1 nN of atomic-scale junctions. An early study[11] revealed the essential features of the mechanical and electrical coupling at nanoscale metallic contacts: the conductance values were significantly less than G_0, the current (I)-voltage (V) characteristics were markedly nonlinear but symmetric about zero bias, and the I-V behavior depended significantly on the contact load, with increasing load leading to increased conductance. Subsequent studies using ultrahigh vacuum (UHV) conducting-probe atomic force microscopy (AFM) or related techniques of metal-metal[12–16] and semiconductor-metal[13,17] nanoscale contacts, in which the insulating barrier material was either adventitious[12,14] or formed deliberately using organic molecular[12,16] or inorganic passivation[15] films, revealed similar behavior: extremely small conductance values and nonlinear I-V behavior indicative of a tunneling mechanism. Here, we extend consideration of nanoscale metal-insulator-metal contacts and demonstrate a method that allows tunneling barrier parameters to be measured as a function of applied contact force. The mechanical measurements are analyzed using the self-consistent Maugis–Dugdale (M-D) contact model.[18] As in previous work, the electrical current is coupled to the contact area extracted from the mechanical analysis, but a parabolic tunneling-barrier conductance model,[19] appropriate to a metal-insulator-metal contact in which the insulator is extremely thin, is used to analyze the electrical measurements.

Mechanical and electrical measurements were performed using an AFM in UHV (base pressure of 5×10^{-8} Pa). The contact electrodes consisted of an atomically smooth Au (111) film on mica and a commercially available Si cantilever with integrated tip coated with about 60 nm of Co followed by 20 nm of Cr (tip radius was ≈ 15 nm). The spring constant of the cantilever in the normal direction was determined to be ≈ 0.12 N m^{-1} using the thermal fluctuation method.[20] The probe was grounded and the sample bias was controlled during the experiments. A typical force-displacement (F-d) trace is shown in Fig. 1. At various points in the retraction cycle, cantilever displacement was halted and I-V measurements performed. The sample bias was swept from -1 to $+1$ V and the current recorded.

The contact area A_c at each of the loads was determined using the M-D contact model. This model perturbs the Hertzian model of spherical contact by imposing a uniform adhesive traction σ in an annular zone of width d exterior to the circular contact radius a. The M-D model can be solved in a self-consistent manner for contact load and displacement of the sphere toward the surface δ. The sphere radius R was taken as the tip radius, and the reduced modulus of the contact, $K = 4/3[(1-\nu^2_{\text{surface}})/E_{\text{surface}} + (1-\nu^2_{\text{probe}})/E_{\text{probe}}]$, was determined using the Young's moduli and Poisson's ratios (E and ν) of Au (80 GPa and 0.42) and Cr (210 GPa and 0.30). Using parameter normalizations of $A = a/(\pi w R^2/K)^{1/3}$, $P = F/\pi w R$, $\Delta = \delta/(\pi^2 w^2 R/K^2)^{1/3}$, S

[a]Author to whom correspondence should be addressed. Electronic mail: frank.delrio@nist.gov.

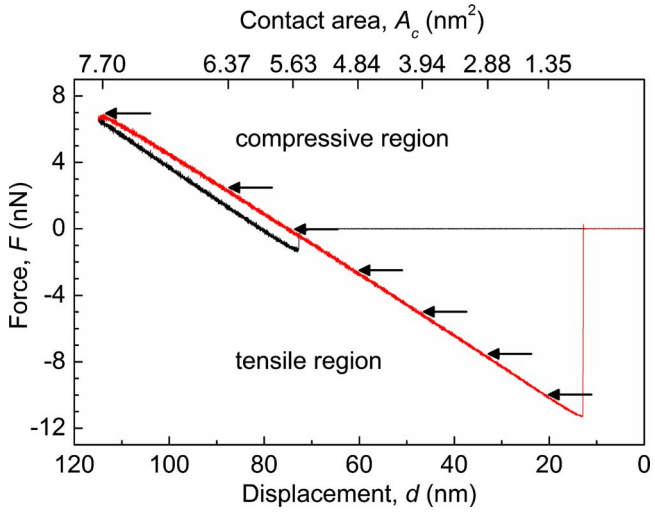

FIG. 1. (Color online) Load-displacement response of Co–Cr AFM tip brought into contact with an Au surface. The arrows indicate loads at which electrical conductance measurements were performed. The tip-surface contact areas at these loads are indicated at the top of the plot.

$=\sigma/(\pi wK^2/8R)^{1/3}$, and $C=[(1+d/a)^2-1]^{1/2}$, the M-D relations for load and sphere displacement are written as

$$P = A^3 - SA^2[C + (C^2+1)\tan^{-1} C], \tag{1}$$

$$\Delta = A^2 - \tfrac{4}{3}SAC, \tag{2}$$

and

$$\tfrac{1}{2}SA^2[C + (C^2-1)\tan^{-1} C] + \tfrac{4}{3}S^2A[C\tan^{-1} C + 1 - (C^2-1)^{1/2}] = 1. \tag{3}$$

Simultaneous solution of Eqs. (1)–(3) at the pull-off load yielded a work of adhesion of $w=120$ mJ m^{-2}. Equations (1)–(3) were then solved using this value of w to determine A_c as a function of F.

Using these contact areas, the variations in current density $J=I/A_c$ with bias were determined for each load as depicted in Fig. 2. I-V behavior was strongly dependent on the

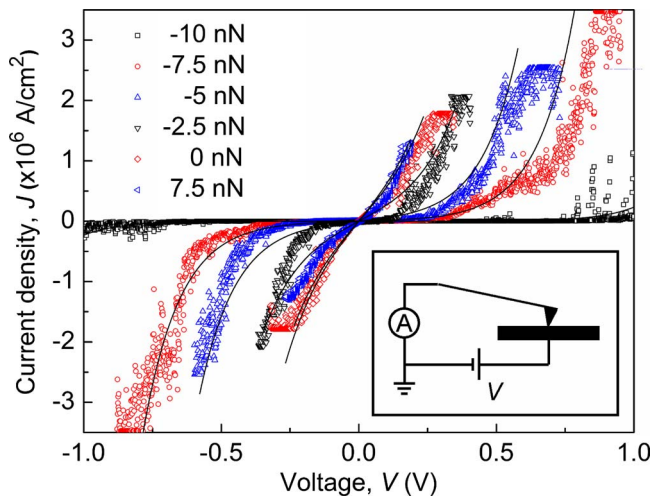

FIG. 2. (Color online) Current density–voltage responses for Cr–Au contacts at the contact loads indicated. Symbols represent measurements for a single voltage sweep. Solid lines represent best fits to the data using a parabolic-barrier tunneling model. The inset is a schematic diagram of the electrical circuit used to obtain the data, showing positive sample bias.

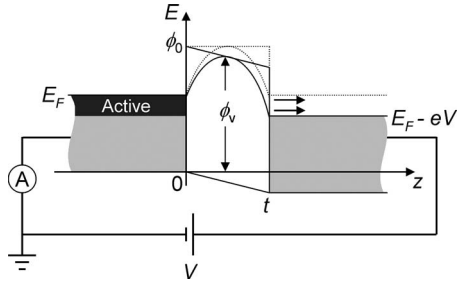

FIG. 3. Schematic diagram of the electron energy levels in metal-insulator-metal structure in which the insulator forms a parabolic barrier for electron tunneling between the metals. The dotted lines indicate the levels in the unbiased state; the solid lines indicate the levels in a biased case (positive if the sample of Fig. 2 is taken on the right).

contact load, with increased contact load leading to increased conductance. In addition, the I-V responses were non-Ohmic, symmetric about zero bias, with conductance values smaller than G_0, which suggests that charge transport involved electron tunneling through an insulating layer. Hansen and Brandbyge[19] developed an approach to describe the I-V characteristics of metal-insulator-metal tunneling junctions. The method assumes a parabolic shape for the tunneling barrier; an energy diagram for a parabolic tunneling barrier is shown in Fig. 3. In the unbiased state, the Fermi energies E_F of the two electrodes are at the same energy level E, whereas in the biased state, the Fermi levels are offset by eV, which enables electrons to travel from left to right through the tunneling barrier. The general formula for current due to tunneling is

$$I = G_S T_m(V) V = \frac{\pi A_c}{\lambda_F^{\,2}} G_0 T_m(V) V, \tag{4}$$

where G_S is the Sharvin conductance, λ_F is the Fermi wavelength, and $T_m(V)$ is the mean transmission probability averaged over all electrons. For very thin barriers and at small voltages, $T_m(V)\approx 1$. Thus, at this extreme, the I-V behavior is described solely in terms of the Sharvin conductance or by $I=G_S V$. The transition to the Sharvin behavior is appropriate, as the contact radius at each load is much less than the mean free path, which is on the order of 10 nm for metals at room temperature.[21] In the presence of a realistic barrier, however, $T_m(V)\ll 1$. Using the Sommerfeld expansion,[21] $T_m(V) \sim T_0(V)+\Delta T(V)$, where $T_0(V)$ is the zero temperature mean transmission and $\Delta T(V)$ is the temperature correction. Using the extended parabolic barrier model,[19]

$$T_0(V) = \frac{1}{\gamma^2 E_F eV}(Li_2\{-\exp[-\gamma(eV+\phi_V-E_F)]\} - Li_2\{-\exp[-\gamma(\phi_V-E_F)]\}) \tag{5}$$

and

$$\Delta T(V) = \frac{\pi^2}{6}\frac{(k_B T)^2}{E_F eV}\left\{\frac{1}{1+\exp[\gamma(\phi_V-E_F)]} - \frac{1}{1+\exp[\gamma(eV+\phi_V-E_F)]}\right\}, \tag{6}$$

where $Li_2(z)$ is the dilogarithm function, k_B is Boltzmann's constant, T is the temperature, $\gamma=(\pi^2 t/h)(2m/\phi_0)^{1/2}$, $\phi_V=\phi_0(1-eV/4\phi_0)^2$ is the voltage-dependent maximum barrier height, m is the mass of an electron, t is the barrier thickness, and ϕ_0 is the zero bias barrier height. Adding Eqs. (5) and (6)

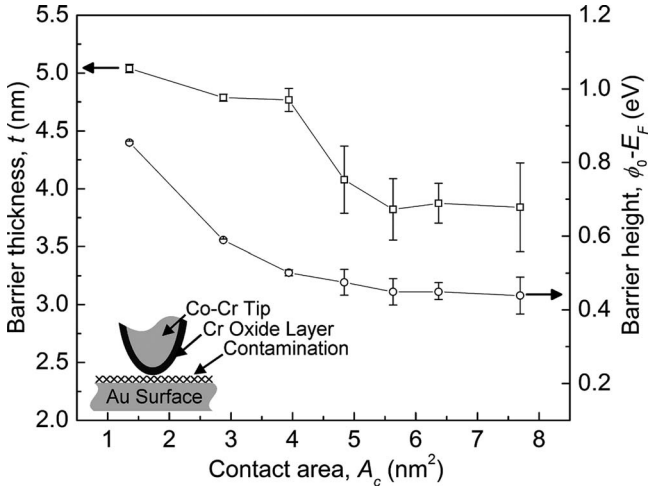

FIG. 4. The variations in tunneling barrier thickness (left) and barrier height (right, in terms of peak energy level above the metal Fermi levels) with contact area of Cr-insulator-Au contacts. The schematic diagram depicts the likely bilayer form of the insulating layer.

and inserting the result into Eq. (4), we arrive at an expression relating the *I-V* behavior to A_c, which can be used in conjunction with Eqs. (1)–(3) to relate the *I-V* data to *F*. As shown in Fig. 2, the parabolic tunneling model (solid lines) was fit to the experimental data (symbols) with good agreement, using *t* and ϕ_0-E_F as the fitting parameters. The resulting values for *t* and ϕ_0-E_F are shown in Fig. 4.

At small A_c, *t* decreased from 5.0 to 3.8 nm, while at larger A_c, *t* remained relatively constant at 3.8 nm. One possible explanation for the change in behavior involves the presence of *two* insulating layers: an oxide layer on the Co–Cr tip and an organic contaminant layer on the Au surface. In this scenario, the probe tip compresses the compliant contaminant layer during the initial stages of contact. Eventually, the contaminant layer is squeezed out from between the contacts, and the insulating layer consists mainly of the oxide layer on the Cr surface, which is more difficult to deform. Organic contaminants are known to rapidly adhere to otherwise "clean" gold surfaces exposed to ambient conditions. Fourier-transform infrared spectroscopy of our Au surface revealed several peaks in the CH stretching region of the spectra. In particular, we identified the CH_2 symmetric mode $\nu_s(CH_2)$ at 2854 cm^{-1}, the CH_2 asymmetric mode $\nu_a(CH_2)$ at 2922 cm^{-1}, and the CH_3 asymmetric in-plane mode, $\nu_a(CH_3,\ \text{ip})$, at 2960 cm^{-1}, which are indicative of disordered, liquidlike organic monolayers.[22] Furthermore, using spectroscopic ellipsometry, the film thickness was found to be 1.3 ± 0.02 nm, assuming a refractive index of $n_f = 1.45$ for the loosely packed hydrocarbon.[22,23] The results are in good agreement with Fig. 4, which suggests a film thickness of 1.2 nm (*t* decreases from 5.0 to 3.8 nm over small values of A_c). Chromium thin films are known to readily form native oxide layers under ambient conditions.[24] In one study, the thickness of the oxide layer varied from 2 to 6 nm, with values depending on the thickness of the chromium thin film and the underlying substrate material.[25] It is reasonable, therefore, to assume that the constant barrier thickness of 3.8 nm at large A_c is due to an oxide layer on the Co–Cr probe tip. As a final note, it is important to point out that the extracted values for ϕ_0-E_F exhibited the same trends as those for *t*; ϕ_0-E_F decreased from 0.85 to 0.45 eV for small A_c and stayed constant at 0.45 eV for large A_c. Lewicki and Mead[26] showed that the potential barrier in a metal-insulator-metal thin film structure increases as the insulator thickness increases, which Simmons[27] later attributed to deep electron traps in the insulating layer.

In summary, we demonstrated a method to extract tunneling barrier parameters of metal-insulator-metal nanoscale contacts. All *I-V* traces exhibited the same sigmoidal shape, with values strongly dependent on the contact load. The barrier thickness and height initially decreased and then remained constant as the contact load increased, presumably due to two different insulating films at the interface.

[1] J. J. Yao, J. Micromech. Microeng. **10**, R9 (2000).
[2] H. A. C. Tilmans, W. De Raedt, and E. J. Beyne, J. Micromech. Microeng. **13**, S139 (2003).
[3] M. Dragoman, A. Takacs, A. A. Muller, H. Hartnagel, R. Plana, K. Grenier, and D. Dubuc, Appl. Phys. Lett. **90**, 113102 (2007).
[4] Y. Cui and C. M. Lieber, Science **291**, 851 (2001).
[5] D. Hyman and M. Mehregany, IEEE Trans. Compon. Packag. Technol. **22**, 357 (1999).
[6] L. L. Mercado, S.-M. Kuo, T.-Y. T. Lee, and L. Liu, Proceedings of the Electronic Components and Technology Conference, 2003 (unpublished), p. 377.
[7] S. T. Patton and J. S. Zabinski, Tribol. Lett. **18**, 215 (2005).
[8] S. Majumder, N. E. McGruer, G. G. Adams, P. M. Zavracky, R. H. Morrison, and J. Krim, Sens. Actuators, A **93**, 19 (2001).
[9] J. I. Pascual, J. Mendez, J. Gomez-Herrero, A. M. Baro, N. Garcia, U. Landman, W. D. Luedtke, E. N. Bogachek, and H.-P. Cheng, J. Vac. Sci. Technol. B **13**, 1280 (1995).
[10] K. Hansen, S. K. Nielsen, M. Brandbyge, E. Laegsgaard, I. Stensgaard, and F. Besenbacher, Appl. Phys. Lett. **77**, 708 (2000).
[11] A. Tonck, F. Houze, L. Boyer, J.-L. Loubet, and J.-M. Georges, J. Phys.: Condens. Matter **3**, 5195 (1991).
[12] J. Beale and F. Pease, IEEE Trans. Compon., Packag. Manuf. Technol., Part A **17**, 257 (1994).
[13] M. A. Lantz, S. J. O'Shea, and M. E. Welland, Phys. Rev. B **56**, 15345 (1997).
[14] J. W. Tringe, T. A. Uhlman, A. C. Oliver, and J. E. Houston, J. Appl. Phys. **93**, 4661 (2003).
[15] M. Enachescu, R. W. Carpick, D. F. Ogletree, and M. J. Salmeron, J. Appl. Phys. **95**, 7694 (2004).
[16] Y. Qi, I. Ratera, J. Y. Park, P. D. Ashby, S. Y. Quek, J. B. Neaton, and M. Salmeron, Langmuir **24**, 2219 (2008).
[17] M. Enachescu, R. J. A. van der Oetelaar, R. W. Carpick, D. F. Ogletree, C. F. J. Flipse, and M. Salmeron, Phys. Rev. Lett. **81**, 1877 (1998).
[18] D. Maugis, J. Colloid Interface Sci. **150**, 243 (1992).
[19] K. Hansen and M. Brandbyge, J. Appl. Phys. **95**, 3582 (2004).
[20] J. L. Hutter and J. Bechhoefer, Rev. Sci. Instrum. **64**, 1868 (1993).
[21] N. W. Ashcroft and N. D. Mermin, *Solid State Physics* (Holt, Rinehart and Winston, New York, 1976).
[22] M. D. Porter, T. B. Bright, D. L. Allara, and C. E. D. Chidsey, J. Am. Chem. Soc. **109**, 3559 (1987).
[23] A. Ulman, *An Introduction to Ultrathin Organic Films: From Langmuir-Blodgett to Self-Assembly* (Academic, New York, 1991).
[24] G. H. Aylward and T. J. V. Findlay, *SI Chemical Data* (Wiley, Sydney, 1974).
[25] R. J. Matyi, M. S. Hatzistergos, and E. Lifshin, Thin Solid Films **515**, 1286 (2006).
[26] G. W. Lewicki and C. A. Mead, Appl. Phys. Lett. **8**, 98 (1966).
[27] J. G. Simmons, Phys. Rev. Lett. **23**, 297 (1969).